Journal of Computer-Aided Molecular Design (2005) 19: 801–820
DOI 10.1007/s10822-005-9028-9

Structure-activity relationships for a new family of sulfonylurea herbicides

Jian-Guo Wang[a], Zheng-Ming Li[a], Ning Ma[a], Bao-Lei Wang[a], Lin Jiang[a], Siew Siew Pang[b,c], Yu-Ting Lee[b], Luke W. Guddat[b,*] & Ronald G. Duggleby[b,*]
[a]*Elemento-Organic Chemistry Institute, State Key Laboratory of Elemento-Organic Chemistry, National Pesticide Engineering Research Center, Nankai University 300071, Tianjin, P R China;* [b]*School of Molecular and Microbial Sciences, The University of Queensland, Brisbane 4072, QLD, Australia;* [c]*Novartis Institute for Tropical Diseases, 10 Biopolis Road #05–01, 138670, Chromos, Singapore*

Received 18 May 2005; accepted 7 November 2005

Key words: 3D-QSAR, acetohydroxyacid synthase, *Arabidopsis thaliana*, computational docking, herbicide, rational drug design, sulfonylurea

Summary

Acetohydroxyacid synthase (AHAS; EC 2.2.1.6) catalyzes the first common step in branched-chain amino acid biosynthesis. The enzyme is inhibited by several chemical classes of compounds and this inhibition is the basis of action of the sulfonylurea and imidazolinone herbicides. The commercial sulfonylureas contain a pyrimidine or a triazine ring that is substituted at both *meta* positions, thus obeying the initial rules proposed by Levitt. Here we assess the activity of 69 monosubstituted sulfonylurea analogs and related compounds as inhibitors of pure recombinant *Arabidopsis thaliana* AHAS and show that disubstitution is not absolutely essential as exemplified by our novel herbicide, monosulfuron (2-nitro-*N*-(4′-methyl-pyrimidin−2′-yl) phenyl-sulfonylurea), which has a pyrimidine ring with a single *meta* substituent. A subset of these compounds was tested for herbicidal activity and it was shown that their effect *in vivo* correlates well with their potency *in vitro* as AHAS inhibitors. Three-dimensional quantitative structure–activity relationships were developed using comparative molecular field analysis and comparative molecular similarity indices analysis. For the latter, the best result was obtained when steric, electrostatic, hydrophobic and H-bond acceptor factors were taken into consideration. The resulting fields were mapped on to the published crystal structure of the yeast enzyme and it was shown that the steric and hydrophobic fields are in good agreement with sulfonylurea-AHAS interaction geometry.

Introduction

The herbicidal activity of sulfonylureas such as *N*-(*p*-cyanophenylaminocarbonyl) benzenesulfonamide (Figure 1) was recognized nearly 40 years ago [1]. Following an extensive synthetic program led by Levitt and colleagues [2] the first modern sulfonylurea herbicide chlorsulfuron (Figure 1) was developed. Since that time, a large number of other sulfonylurea herbicides have been identified and are now used widely [1]. The general features of most active compounds (Figure 1) are an *ortho*-substituted aromatic ring attached to the sulfur atom, and a heterocyclic ring substituted in both *meta* positions and attached to the distal nitrogen atom of the sulfonylurea bridge. This heterocyclic ring is either a pyrimidine (X = CH) or triazine (X = N).

*To whom correspondence should be addressed. Fax: +61-7-3365-4699; E-mail: luke.guddat@uq.edu.au; ronald.duggleby@uq.edu.au

The mode of action of sulfonylureas started to become clear when it was discovered that sulfometuron methyl (Figure 1) is a potent inhibitor of bacterial acetohydroxyacid synthase [3] (AHAS; EC 2.2.1.6), the enzyme that catalyzes the first common step in branched-chain amino acid biosynthesis. Concurrently, Ray showed that chlorsulfuron inhibits plant AHAS [4]. Since then, other sulfonylureas have been shown to inhibit AHAS, and it is widely accepted that inhibition of this enzyme is the mode of action of sulfonylureas as well as several other families of herbicides (see review by Duggleby and Pang) [5]. An important strength of the use of such inhibitors is that there is no AHAS counterpart in humans and other animals.

Understanding the requirement for the common structural features of sulfonylureas (Figure 1) has been held back by the lack of a three-dimensional structure of AHAS. The determination of the structure of the yeast enzyme alone [6], with chlorimuron ethyl (Figure 1) bound [7], and more recently with four other sulfonylurea herbicides bound [8] has now opened the way for comprehending the detailed molecular interactions.

The structure of the yeast AHAS·chlorimuron ethyl complex reveals that the two substituents on the heterocyclic ring (Figure 1; R_2 and R_3) make hydrophobic contacts with the protein. However, the herbicide is involved in numerous other interactions so the requirement for both substituents is not apparent. Removing one of these interactions might weaken binding but it is not obvious why a monosubstituted sulfonylurea would not be herbicidal. Indeed, Li and co-workers have shown that monosulfuron (Figure 1) has herbicidal activity [9]. However, it has not been demonstrated previously that it acts by inhibiting AHAS and it might be a photosynthesis inhibitor, as are the originally described sulfonylureas [2].

Similar to the disubstituted sulfonylurea herbicides, monosulfuron can be used effectively for weed control in a range of crops including wheat, corn, rice, millet and peanut. In particular, monosulfuron is an excellent herbicide in millet fields, where traditional disubstituted sulfonylurea herbicides are non-selective and there are no other effective herbicides currently available [10]. Monosulfuron is also now used as a specific herbicide for *Puccinella tenuiflora*, a weed that is commonly observed in the alkali soil of northern China where it drastically affects the yield of wheat crops grown in these areas.

Here we show that monosulfuron inhibits pure recombinant *Arabidopsis thaliana* AHAS. Its activity as an inhibitor is characterized, together with that of 68 other sulfonylurea analogs, and 10 commercial sulfonylurea herbicides. Three-dimensional quantitative structure–activity relationships (3D-QSAR) are developed that account well for the potency of inhibition. The resulting fields were mapped on to the herbicide-binding site of yeast AHAS, and it was shown that the steric and hydrophobic fields were in good agreement with sulfonylurea-AHAS interaction geometry. The models highlight the important structural requirements of herbicidal sulfonylureas and provide new clues for the design of molecules with enhanced bioactivities. The herbicidal activity of 24 monosubstituted sulfonylureas was tested against the growth of rape seeds (*Brassica napus*), which has an AHAS that is 93% identical to that of *A. thaliana* AHAS, and where there is 100% conservation of the active site residues. The results show that the inhibitory power of these sulfonylureas against *A. thaliana* AHAS correlates well with their potency as rape seed herbicides.

Experimental methods

Synthesis of sulfonylurea analogs

Most of the compounds were synthesized using one of the two following procedures that are detailed by Li and colleagues [9, 11, 12]. The complete synthesis and characterization of the other compounds will be described elsewhere.

AHAS expression and purification

The AHAS expression plasmid used here is a modification of that described previously [12]. The DNA sequence encoding the mature enzyme (after removal of the chloroplast transit peptide) was subcloned into the pET30a(+) vector to introduce a C-terminal hexahistidine tag [13]. This plasmid was used to transform *Escherichia coli* strain BL21(DE3) cells, and the cells were grown at 37 °C in 2YT medium [14] containing 50 μg/mL kanamycin. When the OD_{600} reached 0.8 to 1.0, expression was induced with 1.0 mM IPTG and cells were incubated for 4 to 5 h at room temperature (~22 °C). Cells were harvested by centrifugation and stored at −20 °C.

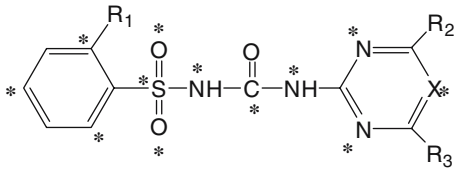

General structure for sulfonylurea herbicides

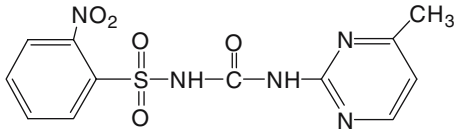

monosulfuron

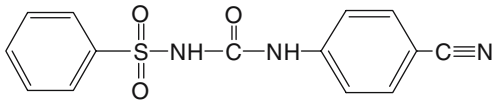

N-(*p*-cyanophenylaminocarbonyl)benzenesulfonamide

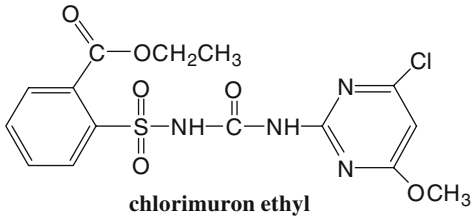

chlorimuron ethyl

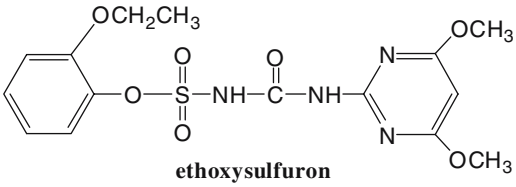

ethoxysulfuron

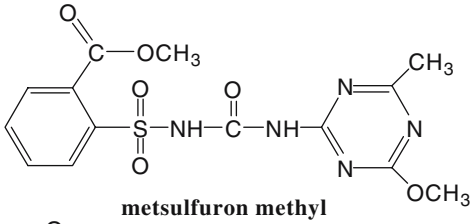

metsulfuron methyl

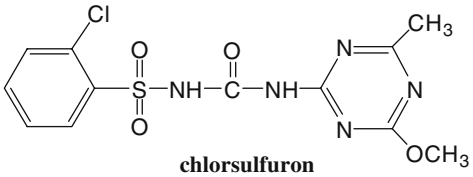

chlorsulfuron

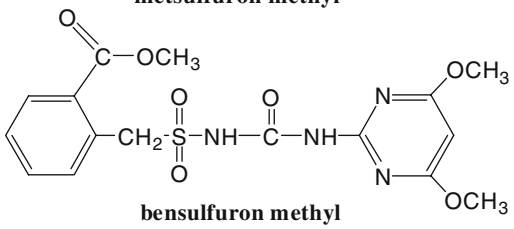

bensulfuron methyl

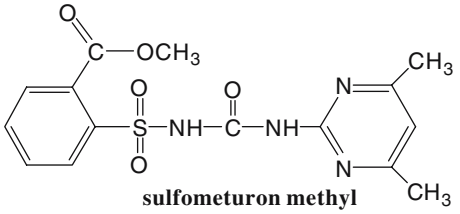

sulfometuron methyl

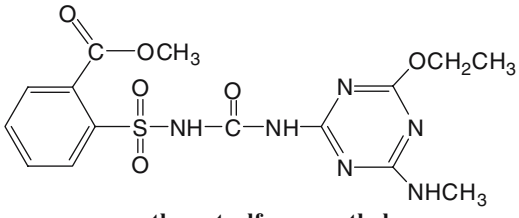

ethametsulfuron methyl

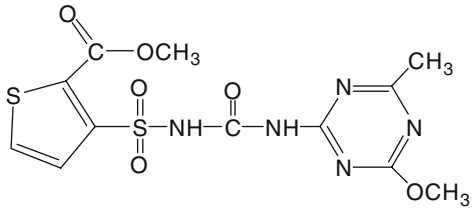

thifensulfuron methyl

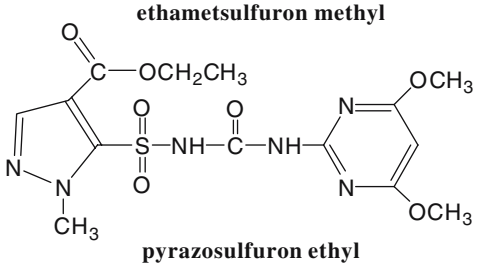

pyrazosulfuron ethyl

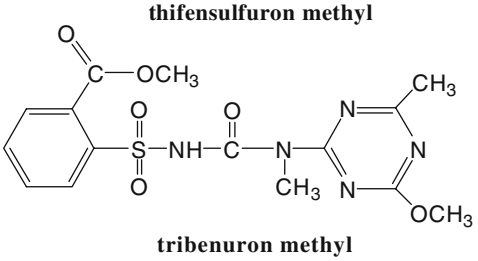

tribenuron methyl

Figure 1. Sulfonylurea herbicide structures. In the general structure, the atoms labeled with asterisks were used to overlay different structures for 3D-QSAR studies. Also shown are monosulfuron and *N*-(*p*-cyanophenylaminocarbonyl)benzenesulfonamide and the complete structures of 10 disubstituted sulfonylurea herbicides used in this study.

All subsequent operations were performed at 4 °C, excluding light wherever possible. Thawed cells were resuspended in buffer (500 mM NaCl, 20 mM Tris–Cl (pH 7.9), 10 μM FAD) containing 5 mM imidazole, using approximately 5 mL per g wet weight of cells. Lysozyme (10 mg per g of cells) was added and lysis was carried out on ice for 30 min. After sonication (5×20 s with 1 min rest intervals), the lysate was clarified by centrifugation and filtered through a 0.45 μm membrane.

The hexahistidine-tagged AHAS was purified by immobilized nickel affinity chromatography using Novagen His·Bind metal chelation resin. After applying the clarified lysate, the column was washed with 3 volumes of 5 mM imidazole in buffer and 3 volumes of 25 mM imidazole in buffer. The enzyme was then eluted with 6 volumes of 400 mM imidazole in buffer. The solvent was changed to 10 μM FAD, 5 mM DTT and 15% (v/v) glycerol in 50 mM potassium phosphate (pH 7.0) by gel filtration, and the purified enzyme was stored in small aliquots at −70 °C.

AHAS assays

AHAS activity was measured using the colorimetric assay as described previously [13] in 50 mM potassium phosphate (pH 7.0) containing 50 mM pyruvate, 1 mM thiamine diphosphate, 10 mM $MgCl_2$, and 10 μM FAD. After incubation for 30 min at 37 °C, acetolactate was estimated [15].

Measurement of inhibition constants

Trial experiments with a wide range of inhibitor concentrations were used to establish a suitable concentration window. Subsequently, AHAS activity was measured at a series of inhibitor concentrations within this window. Usually, a total of 12 concentrations were used (including no inhibitor), in duplicate. The data were analyzed by nonlinear regression using Equation 1 to estimate the values and standard errors for the apparent inhibition constant (K_i^{app}) and the uninhibited rate (v_o).

$$v = v_o/(1 + [I]/K_i^{app}) \quad (1)$$

Some compounds gave less than 50% inhibition at the highest concentration tested (usually 400 μM). Where the observed inhibition was in the range 15 to 40%, an approximate K_i^{app} was estimated from Equation 1 and the highest inhibitor concentration tested. If the observed inhibition was less than 15%, Equation 1 was used to place a lower limit on the value of K_i^{app} of nine times the highest inhibitor concentration tested (i.e. assuming that the inhibition is 10% or less).

In a few cases, there appeared to be a small residual activity (v_∞) at high [I] so the data were re-analyzed using Equation 2.

$$v = (v_o - v_\infty)/(1 + [I]/K_i^{app}) + v_\infty \quad (2)$$

The resulting values for K_i^{app} obtained using Equation 1 or 2 were usually similar and typically differed by approximately 20%.

Measurement of herbicidal activity

The method was adapted from that described elsewhere [16]. Rape seeds were obtained from a local market in Tianjin, P.R. China. The compounds to be tested were made into an emulsion to aid dissolution. Seeds were soaked in distilled water for 4 h before being placed on a filter paper in a 6-cm Petri plate, to which 2 mL of inhibitor solution had been added in advance. Usually, 15 seeds were used on each plate. The plate was placed in a dark room and allowed to germinate for 48 h at 28 ± 1 °C. The lengths of 10 rape roots selected from each plate were measured and the means were calculated. Preliminary screening of a broad range of inhibitor concentrations was used to identify a narrow concentration window where inhibition of root growth occurred. Subsequently, a series of six to nine different concentrations within this window were used in duplicate, plus a control without inhibitor. Generally, the ratio between successive concentrations in the series was 2.0 or 2.5.

Calculation of IC_{50} values

The average length of the roots for each trial was used to calculate a percent inhibition, relative to the control with no added inhibitor. These values were converted to probits using a standard statistical table. Weights were calculated in proportion to the inverse of the variance of the 10 probit

values obtained from the replicate measurements. The IC_{50} is the inhibitor concentration that gives a probit of 5. Therefore, the data were then analyzed by weighted nonlinear regression using Equation 3 (below) to give the best fit values and standard errors for the slope (m) and the IC_{50}

$$\text{Probit} = m(\log[I] - \log[IC_{50}]) + 5 \quad (3)$$

Molecular modeling of ligand structure, minimization and alignment

The 3D structure of each sulfonylurea was built and modeled in SYBYL6.9 (Tripos Associates, St. Louis, MO) on an SGI Origin 350 server (R16000) and workstation (R4000). All structures were constructed based on the conformation of chlorimuron ethyl in complex with yeast AHAS. The conformations of the AHAS inhibitors were further adjusted by molecular mechanics to refine bond lengths and angles using the Tripos force field and Gasteiger–Hückel charges. A nonbond cutoff of 8 Å was utilized in the structural optimization to consider the intramolecular interactions. The minimization terminated at an energy convergence of 0.005 kcal mol^{-1} $Å^{-1}$. All compounds were superimposed upon chlorimuron ethyl to match the atoms in common (labeled with asterisks in Figure 1).

3D-QSAR analysis

CoMFA and CoMSIA studies were performed with the 3D-QSAR module of SYBYL. The same alignment was subjected to both 3D-QSAR investigations. The CoMFA steric and electrostatic fields and the CoMSIA steric, electrostatic, and hydrophobic and H-bond donor and acceptor fields were calculated within a grid lattice with a resolution of 2 Å. The extension was 10 Å beyond every molecular boundary in every direction. An sp^3 carbon probe atom with a positive charge was used to generate the interaction energies at each lattice point. For CoMFA, the steric and electrostatic contributions were truncated to 30 kcal/mol; for CoMSIA, the five similarity-index fields were calculated when the attenuation factor was set to a value of 0.3.

3D-QSAR equations were derived by partial least squares (PLS) analysis using the ''Leave-One-Out'' method to perform cross-validation. Prior to the PLS analysis, CoMFA or CoMSIA columns with a variance smaller than 2.0 kcal/mol were filtered to improve the signal-to-noise ratio. The optimal number of components was selected as providing the highest cross-validated q^2 value (Equation 4). Subsequently, non-cross-validated analysis was carried out to calculate the conventional r^2, the variance ratio (F) and the standard error values (s, Equation 5) using the optimum number of components. Finally, the 3D-QSAR models were produced from the non-cross-validated calculations and the results were graphically interpreted by field contribution plots.

$$q^2 = 1 - \Sigma(Y_{obs} - Y_{pred})^2 / \Sigma(Y_{obs} - Y_{mean})^2 \quad (4)$$

$$s^2 = \Sigma(Y_{obs} - Y_{calc})^2 / (m - k - 1) \quad (5)$$

In these equations, Y_{obs}, Y_{pred} and Y_{calc} are the observed values of pK_i^{app}, predicted values of pK_i^{app} from cross-validated analysis and calculated values of pK_i^{app} from non-cross-validated analysis. Y_{mean} is the mean value of Y_{obs} within the data set, m is the number of compounds and k is the number of PLS factors. ''Std. dev*coeff'' was used to represent the graphical results in CoMFA and CoMSIA fields. Threshold values selected were 80% for favored regions and 20% for unfavored regions.

Results and discussion

Inhibition of AHAS by commercial disubstituted sulfonylureas

Previously we [17] have characterized the inhibition of pure recombinant *A. thaliana* AHAS by six commercial sulfonylureas (Table 1). The recombinant enzyme used in those studies consisted of the presumed mature protein after deletion of the first 85 residues constituting the chloroplast transit peptide. The recombinant enzyme used here is similar, except that it was engineered to include an eight-residue C-terminal peptide containing a hexahistidine tag to simplify purification. The potency of the inhibitors is similar (Table 1), showing that the addition of the affinity tag to the protein has no major influence on its susceptibility to sulfonylureas. These commercial sulfo-

Table 1. Inhibition of *A. thaliana* AHAS by commercial sulfonylurea herbicides[a].

Herbicide	K_i^{app} (nM)	
	This study	Literature [17]
chlorimuron ethyl	8.3 ± 0.4	10.8 ± 1.3
ethoxysulfuron	8.9 ± 0.4	
metsulfuron methyl	10.7 ± 0.7	36.2 ± 1.9
chlorsulfuron	14.4 ± 1.0	54.6 ± 4.8
bensulfuron methyl	16.2 ± 0.4	
sulfometuron methyl	39.5 ± 2.6	25.5 ± 4.1
ethametsulfuron methyl	52.2 ± 2.2	
thifensulfuron methyl	60.1 ± 2.0	72.2 ± 4.3
pyrazosulfuron ethyl	101 ± 3	
tribenuron methyl	316 ± 21	253 ± 12

[a]Structures are illustrated in Figure 1.

nylureas inhibit with apparent inhibition constants in the range of 10 to 300 nM; the four compounds that we have not tested previously on the recombinant *A. thaliana* AHAS also have inhibition constants that fall within this range.

Inhibition of AHAS by monosubstituted sulfonylureas

A. thaliana AHAS is inhibited (Figure 2) by monosulfuron (Figure 1) with an apparent inhibition constant of 245 nM (compound **1**, Table 2). It is less potent than most of the commercial disub-

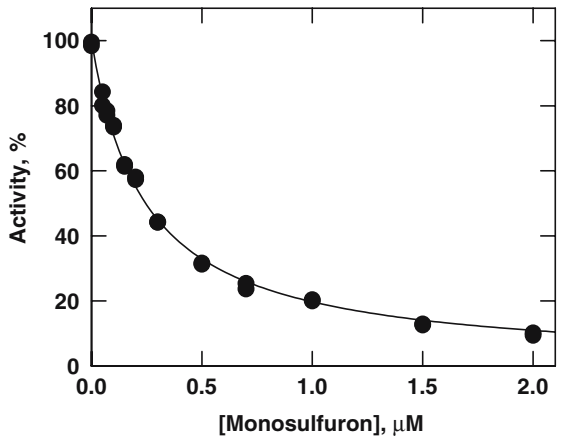

Figure 2. Inhibition of *A. thaliana* AHAS by monosulfuron. Activity was measured over a range of monosulfuron concentrations. Duplicate measurements are too similar to be visible as separate points in most cases. The data were fitted using Equation 1 and are plotted after normalizing to an uninhibited rate of 100%.

Table 2. Inhibition of *A. thaliana* AHAS by monosubstituted sulfonylureas[a].

Compound	R_1	R_2	K_i^{app} (μM)
1	NO_2	CH_3	0.245 ± 0.007
2	$COOC_2H_5$	CH_3	0.266 ± 0.012
3	$COOCH_3$	CH_3	0.363 ± 0.017
4	$COOC_2H_5$	OCH_3	0.488 ± 0.035
5	$COOC_2H_5$	Cl	0.645 ± 0.042
6	NO_2	C_2H_5	0.779 ± 0.056
7	NO_2	OC_2H_5	1.10 ± 0.07
8	$COOCH_2CH_2Cl$	CH_3	1.21 ± 0.08
9	$COOCH(CH_3)_2$	CH_3	1.26 ± 0.06
10	$COOCH(CH_3)_2$	OCH_3	1.31 ± 0.11
11	$COOCH_2CH_2Cl$	OCH_3	1.41 ± 0.08
12	NO_2	SCH_3	1.76 ± 0.16
13	$COOC_2H_5$	OC_2H_5	2.07 ± 0.17
14	$COOCH_2$phenyl	OCH_3	2.24 ± 0.12
15	NO_2	$CH(CH_3)_2$	2.99 ± 0.58
16	$COOCH_3$	SCH_3	3.24 ± 0.19
17	Cl	OCH_3	5.37 ± 0.50
18	$COOCH_2$phenyl	CH_3	8.33 ± 0.54
19	$COOC_2H_5$	$OCH(CH_3)_2$	11.3 ± 0.8
20	$COOCH_3$	OC_2H_5	12.3 ± 0.5
21	$COOCH_2C_6H_{11}$ [b]	CH_3	13.0 ± 0.5
22	$COOCH_3$	OC_3H_7	13.7 ± 1.0
23	$COOCH_2C_6H_{11}$ [b]	OCH_3	15.1 ± 1.0
24	$COOC_2H_4OC_2H_5$	CH_3	15.8 ± 1.0
25	$COOC_2H_4OC_2H_5$	OCH_3	25.1 ± 1.3
26	$COOCH_3$	OCH_2CH_2F	30.2 ± 1.7
27	NO_2	H	32.7 ± 5.4
28	$COOCH_3$	H	32.9 ± 1.8
29	Cl	OC_2H_5	37.4 ± 3.7
30	$NHCOCF_3$	CH_3	51.3 ± 2.3
31	$COOC_2H_5$	SC_2H_5	51.5 ± 3.3
32	$NHCOCF_3$	OCH_3	56.6 ± 5.2
33	NO_2	SC_2H_5	90.3 ± 8.6
34	$NHCOCF_3$	OC_2H_5	101 ± 18
35	$COOC_2H_4OCH_3$	OCH_3	195 ± 12
36	$COOC_2H_5$	$NHCH_3$	228 ± 12
37	$COOC_2H_4OCH_3$	CH_3	372 ± 25
38	$COOC_2H_5$	$N(CH_3)_2$	375 ± 68
39	NO_2	$NHCH_3$	~600
40	$COOC_2H_5$	$OC_2H_4OCH_3$	~1600
41	$COOCH_3$	SC_3H_7	> 2160
42	$COOC_2H_5$	$OC_2H_4OC_2H_5$	~2300
43	$COOCH_3$	SC_2H_5	>2880
44	$COOCH_3$	$OC_2H_4OCH_3$	>3600
45	$COOCH_3$	$OC_2H_4OC_2H_5$	>3600

[a]Structures are as illustrated in Figure 1, with R_3 = H and X = CH.
[b]C_6H_{11} represents a cyclohexyl group.

stituted sulfonylureas tested, but has a similar apparent inhibition constant to that of tribenuron methyl. This compound is used to kill broadleaf weeds in cereal crops at application rates of 5 to 30 g/ha, similar to those used for other sulfonylureas [18]. Thus, on the basis of its potency *in vitro*, we expect that monosulfuron would be an effective herbicide. Table 2 also lists the inhibition constants of a further 44 monosubstituted sulfonylureas that conform to the general structure of Figure 1 (X = CH, R_3 = H), listed in order of potency. As described later, the potencies of these and a further 24 related compounds (see below) were subjected to 3D-QSAR analysis.

Sulfonylurea bridge modifications

Three of the commercial sulfonylureas listed in Table 1 have modifications to the bridge connecting the aromatic and heterocyclic rings. Bensulfuron methyl has a methylene group in the bridge (see Figure 3a; Y = CH_2) while ethoxysulfuron has an oxygen atom in this position. Finally, tribenuron methyl has a methyl group in the Z position. Fifteen monosubstituted analogs of these compounds were tested (Figure 3b). All of them proved to be very weak inhibitors with the strongest (compound **46**) being more than 250-fold less potent than the weakest of the commercial herbicides (tribenuron methyl). Clearly, the combination of bridge modifications with a monosubstituted heterocyclic ring is detrimental for binding to AHAS.

Pyrazoles, pyridines and thiazoles

The herbicide pyrazosulfuron ethyl has a substituted pyrazole ring in place of the normal aromatic ring (Figure 3c; R_2 = R_3 = OCH_3). Four monosubstituted analogs were tested as AHAS inhibitors (Figure 3d). Two of these compounds (**61** and **62**) are moderately strong inhibitors with apparent K_i values of around 25 μM, although these values are substantially higher than that for pyrazosulfuron ethyl (0.1 μM). Five other compounds, three pyridines with a truncated bridge and two thiazoles (Figure 4), were tested but none is a strong inhibitor of AHAS. This is not surprising in view of their substantial structural differences from conventional sulfonylureas.

3D-QSAR analyses

Previously published 3D-QSAR analyses of sulfonylurea herbicides [19–26] suffer from several shortcomings. Firstly, the assumed bioactive conformation was based on either the structures of sulfonylureas crystallized as free molecules [20–23, 25] or their low energy conformers calculated theoretically [19, 24, 26]. However, it is now known that none of these conformations match that observed when a sulfonylurea is bound to its target enzyme [7,8]. Secondly, most activity data employed in previous QSAR investigations were obtained using *in vivo* experiments [19–26]. Herbicidal activity depends ultimately upon inhibition of AHAS, but there are differences between *in vivo* and *in vitro* effects of these compounds due to barriers between the site of application and the intracellular target, degradation and detoxification by the plant, and so on. Thirdly, the structure of the herbicide-binding site was not known at the time, so it was not clear what specific interactions were being made to inhibit AHAS. Finally, although some QSAR models demonstrate graphically the putative binding mode [19], biophore [24] or stereoelectronic properties [26] of this family of herbicides, these models lack the ability to predict the biological activity of new compounds. We are now in a position to correct these deficiencies.

The publication of the crystal structure of yeast AHAS with bound chlorimuron ethyl [7], and with four other members of the sulfonylurea family [8] has allowed the elucidation of the herbicide-binding site of AHAS. This has also defined the bioactive conformation and provided insights into the exact molecular interactions of this category of herbicides. Further, as described above we have measured the apparent inhibition constants against a pure plant AHAS of 69 sulfonylureas with a single *meta* substituent, as well as the inhibition by 10 commercial disubstituted sulfonylurea herbicides. The apparent inhibition constants of the sulfonylureas tested span the range from 10^{-9} M to 10^{-3} M. These data provide for the first time an extensive and accurate data set that is not influenced by *in vivo* effects unrelated to the primary enzyme-inhibitor interaction. These experimental advances now allow us to establish new correlations between the functions and structural characteristics, and to develop new 3D-QSAR models to

elucidate necessary molecular features for this family of herbicides.

We have used comparative molecular field analysis (CoMFA [27]) and comparative molecular similarity indices analysis (CoMSIA [28]) for constructing 3D-QSAR models. Both methods are based on the assumption [29] that changes in binding affinities of ligands are related to changes in the molecular field properties. CoMFA samples the steric and electrostatic fields surrounding a training set of ligands and constructs a 3D-QSAR model by correlating these fields with the observed activities. CoMSIA considers five different fields: steric, electrostatic, hydrophobic, H-bond donor and H-bond acceptor. CoMFA uses Lennard–Jones and Coulombic potential to calculate the fields while CoMSIA utilizes a Gaussian function for these calculations.

(a)

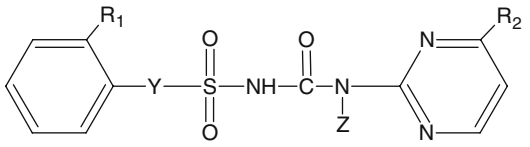

(b)

Compound	R_1	R_2	Y	Z	K_i^{app}, μM
46	$CO\,OCH_3$	CH_3	CH_2	H	84.8 ± 3.0
47	$CO\,OCH_3$	$NHCH_3$	CH_2	H	94.3 ± 3.3
48	$CO\,OCH_3$	OCH_2CH_3	CH_2	H	143 ± 4
49	$CO\,OCH_3$	CH_3	O	H	132 ± 9
50	$CO\,OCH_3$	C_2H_5	O	H	191 ± 23
51	OCH_3	CH_3	O	H	187 ± 25
52	NO_2	CH_3	-	C_4H_9	270 ± 47
53	NO_2	CH_3	-	$(C_2H_5)CHCH_3$	373 ± 60
54	NO_2	CH_3	-	CH_3	~600
55	$CO\,OC_2H_5$	CH_3	-	CH_3	~900
56	$CO\,OCH_3$	CH_3	-	CH_3	>3600
57	$CO\,OCH_3$	CH_3	-	C_4H_9	>3600
58	$CO\,OCH_3$	CH_3	-	$(C_2H_5)CHCH_3$	>3600
59	$CO\,OC_2H_5$	CH_3	-	C_3H_7	>3600
60	$CO\,OC_2H_5$	CH_3	-	C_5H_{11}	>3600

(c)

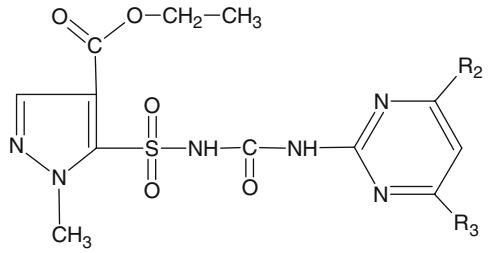

(d)

Compound	R_2	R_3	K_i^{app}, μM
61	CH_3	H	22.5 ± 2.7
62	OCH_2CH_3	H	31.5 ± 2.1
63	SCH_3	H	184 ± 11
64	$NHCH_3$	H	>3600

Figure 3. Inhibition of *A. thaliana* AHAS by atypical monosubstituted sulfonylureas. Panel (a) shows general structure of the monosubstituted sulfonylureas with modifications in the bridge while the inhibition constants of those compounds that were tested are shown in panel (b). Panel (c) shows general structure of a pyrazole sulfonylurea while the inhibition constants of those compounds that were tested are shown in panel (d).

Determination of bioactive conformations

To perform 3D-QSAR analysis it is important to identify the biologically active conformer of a ligand [29]. The binding mode and conformation of chlorimuron ethyl interacting with yeast AHAS (PDB code 1N0H) was used as a template to construct all molecules under investigation. It should be noted that the inhibition data were obtained using *A. thaliana* AHAS while the structure of yeast AHAS is utilized to interpret the results. However, the *A. thaliana* AHAS-chlorimuron ethyl complex has been successfully crystallized [30] and refinement of that structure (unpublished data) indicates that the sulfonylurea has a similar binding geometry. Consistent with this observation, the potency of inhibition by sulfonylureas is similar between yeast AHAS [31] and *A. thaliana* AHAS [17]. Furthermore, the amino acids that line the sulfonylurea-binding site

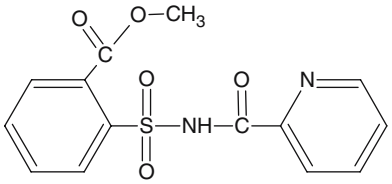

65 $K_i^{app} = 200 \pm 40\ \mu M$

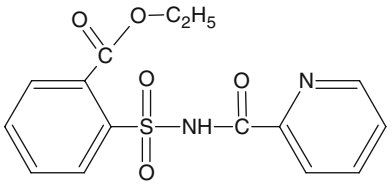

66 $K_i^{app} \sim 600\ \mu M$

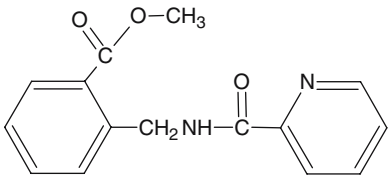

67 $K_i^{app} > 3600\ \mu M$

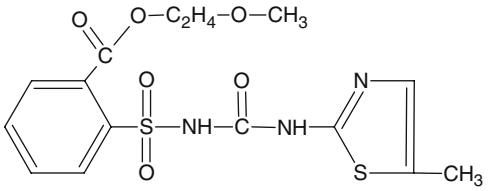

68 $K_i^{app} = 319 \pm 21\ \mu M$

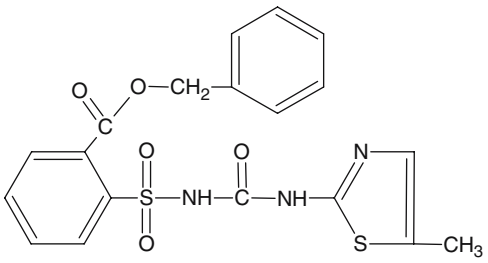

69 $K_i^{app} \sim 1200\ \mu M$

Figure 4. Inhibition of *A. thaliana* AHAS by pyridines and thiazoles. The structures of the compounds are shown in the left column, while their inhibition constants are shown in the right column.

of the two enzymes are highly conserved. Thus, the structure of yeast AHAS represents a high-quality model of the plant enzyme.

Data set and alignment rule

A panel of 68 sulfonylureas selected from those described earlier was used to examine the relationship between the inhibition data and the molecular physicochemical descriptors. These compounds included the 10 commercial sulfonylureas shown in Table 1, and all of the 69 compounds shown in Table 2, Figure 3, and Figure 4, apart from 11 (**41**, **43**, **44**, **45**, **56**, **57**, **58**, **59**, **60**, **64** and **67**) for which an accurate K_i^{app} value was too high to be determined. The biological activity used here was expressed as pK_i^{app} (i.e. $-\log_{10} K_i^{app}$). In this report the data have been subjected to three different analyses: For Group 1, a set of 15 molecules chosen at random (**2**, **6**, **10**, **16**, **20**, **27**, **35**, **49**, **51**, **53**, **54**, **69**, chlorsulfuron, sulfometuron methyl and pyrazosulfuron ethyl) made up a test set, while the remaining 53 sulfonylureas were treated as the training set. The test set was used to validate the predictive ability of the model derived from the training set. The robustness of the predictive power was therefore assessed. For Group 2, the commercial sulfonylureas were omitted to leave 58 monosubstituted sulfonylureas. These formed a training set to produce 3D-QSAR models for the design of more potent monosubstituted sulfonylureas. For Group 3, the whole set of 68 molecules was used to derive the most comprehensive 3D-QSAR analysis to date.

The alignment rule [29] used to superimpose the inhibitors under study is an important factor in the quality of 3D-QSAR. Atom-by-atom fit and field fit are the two basic methods used to superimpose diverse molecules. When the structure of the binding site is known, molecular docking is another way to guide the alignment. We have tried docking all of the sulfonylureas into the binding site of yeast AHAS. All molecules were initially docked successfully but their predicted conformations were not consistent with the known location of chlorimuron ethyl in yeast AHAS [7]. Therefore, the corresponding alignment could not be used for the subsequent 3D-QSAR analysis. Instead, all 68 compounds were superimposed on chlorimuronethyl as rigid bodies. Most of the sulfonylureas with classic structures (Figure 1) were fitted based upon the core set of atoms (those labeled with asterisks). For those with a lengthened or shortened sulfonylurea bridge, or with atypical ring structures, the maximum common structure was fitted to the template. Thus, for 46–51, the benzyl ring was not superimposed while for 65–67 the pyrimidine ring was not included in the superimposition. It should be noted that a single substituent on the heterocycle may be placed in either the R_2 or R_3 positions (Figure 1). Preliminary analysis of the monosulfuron–*A. thaliana* AHAS complex crystal structure (unpublished data) has revealed that the substituent is located in the same position as the chlorine atom in chlorimuron ethyl. Accordingly, all monosubstituted sulfonylureas were aligned in this manner. Where the disubstituted sulfonylureas differed in the substituent at R2 and R3, the choice of which substitutent occupied these positions was based on the conformer that had the lowest energy in the SYBYL calculations. For chlorimuron ethyl, tribenuron methyl, chlorsulfuron and metsulfuron methyl, these calculations gave the same conformation as observed in the crystal structures of the yeast AHAS complexes [8]. The superposition of all sulfonylureas is shown in Figure 5.

CoMFA and CoMSIA studies

Starting from the structural alignment of Figure 5, comprehensive CoMFA and CoMSIA analyses were performed and their respective models were developed. Comparison of experimental and predicted activities by CoMFA and CoMSIA for all of the compounds in this study is presented in Table 3. The cross-validated results were assessed by their q^2 value (see Experimental Methods), where a value above 0.3 indicates that the probability of chance correlation is less than 5% and a value over 0.5 is highly significant. The results of these computations are summarized in Tables 4 and 5. For Group 1, CoMFA analysis exhibited a cross-validated q^2 of 0.459 and non-cross-validated r^2 of 0.966. This high degree of agreement between the calculated and experimental inhibition constants is illustrated in Figure 6a. The predictive ability of this model was demonstrated by the r^2_{pred} of 0.687 for the external test set of 15 molecules (Figure 6b). The model is relatively good, especially given that the structures of the molecules in the database are quite diverse. No compounds

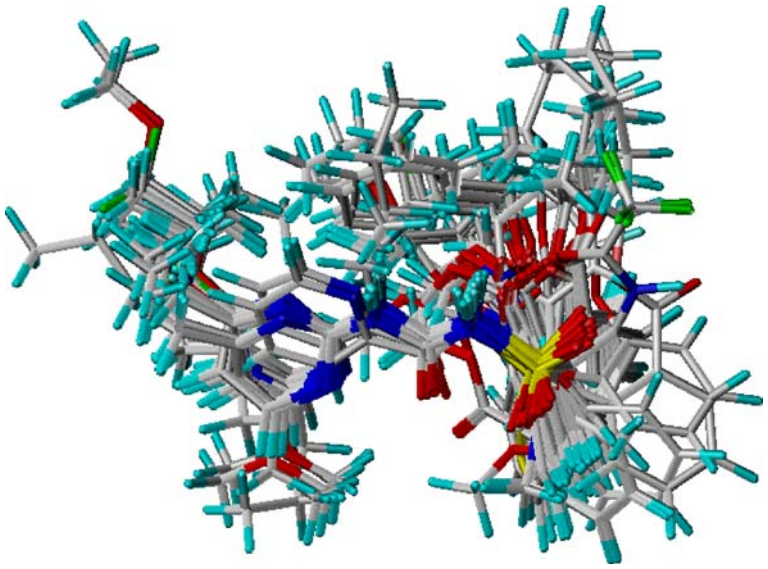

Figure 5. Superimposition of 68 sulfonylureas for 3D-QSAR studies from the rigid fit alignment rule. The conformation of chlorimuron ethyl in complex with yeast AHAS was used as a template.

from the list had to be omitted though three were poorly predicted by this cross validation method and considered as outliers. Nonetheless, inclusion of these in the calculations still gave a satisfactory q^2 value. The results indicate that the conformer selection and alignment rule described previously are reasonable. Because most of the sulfonylureas have only one substituent on the heterocyclic ring, the Group 2 3D-QSAR study focused on this monosubstituted series of sulfonylureas. A cross-validated q^2 of 0.611 with 8 partial least squares (PLS) components was reached, while the conventional r^2 has a high value of 0.959 (Figure 6c). The full data set of Group 3 resulted in a best q^2 of 0.673, for 8 PLS components and a non-cross validated r^2 of 0.974 (Figure 6d). For both groups when the number of PLS components was less than 8, the cross-validated q^2 value decreased significantly. For all CoMFA, steric effects contributed slightly more than electrostatic fields (Table 4).

Although CoMFA is sometimes superior to CoMSIA analysis it has the disadvantage (in our version of the Sybyl software) that it does not assess hydrophobic interactions and H-bonds, key features of inhibitor-enzyme interactions. To overcome this CoMSIA analysis was also conducted on Group 2 and Group 3. Various arrangements of the five possible fields resulted in 31 combinations (Table 5). For Group 2, the cross-validated q^2 varied over the range 0.273 to 0.458, a result that is on the borderline of acceptability. Among the 31 combinations for Group 3, 20 analyses yielded q^2 values above 0.5. A best q^2 of 0.644 was observed at 8 PLS components when steric, electrostatic, hydrophobic and H-bond acceptor fields were included in the combination. In order to explain the hydrophobic and H-bond fields, this case was used to generate CoMSIA models for the sulfonylureas. A non-cross-validated r^2 of 0.931 indicated that the final CoMSIA model was highly self-consistent. For the CoMSIA analysis, the contributions from the various fields were 21.5% steric, 32.4% electrostatic, 33.8% hydrophobic and 12.3% H-bond acceptor (Table 4). The steric component of the CoMFA model partitions between steric and hydrophobic in the CoMSIA model, while the electrostatic component of CoMFA is split into the CoMSIA electrostatic and H-bond acceptor components. The calculated *versus* observed activity for this CoMSIA model of the sulfonylureas is shown in Figure 6e.

Structure-based interpretation of 3D-QSAR models

Although structure-based design approaches are focused towards a detailed understanding of protein–ligand interactions, they do not always provide the ability to predict the activity of a novel analogue. On the other hand, complementary statistical 3D-QSAR methods cannot be interpreted in protein

Table 3. Experimental and predicted biological activities of 3D-QSAR (using cross-validation).

Compound[a]	Experimental pK_i^{app}	Group 1 CoMFA		Group 2 CoMFA		Group 3 CoMFA		Group 3 CoMSIA	
		pK_i^{app}	Residual	pK_i^{app}	Residual	pK_i^{app}	Residual	pK_i^{app}	Residual
1	6.61	6.26	0.35	6.05	0.56	6.02	0.59	5.62	0.99
2	6.57	TS[b]	TS[b]	5.40	1.17	5.33	1.24	5.61	0.96
3	6.44	4.77	1.67	5.34	1.10	5.61	0.83	5.42	1.02
4	6.31	5.91	0.40	6.08	0.23	5.81	0.50	5.10	1.21
5	6.19	5.67	0.52	5.59	0.60	5.61	0.58	5.99	0.20
6	6.11	TS[b]	TS[b]	6.15	−0.04	6.06	0.05	5.45	0.66
7	5.96	5.96	0.00	5.66	0.30	5.73	0.23	5.26	0.70
8	5.92	5.70	0.22	5.91	0.01	5.95	−0.03	6.11	-0.19
9	5.90	5.82	0.08	6.18	−0.28	6.10	−0.20	6.34	−0.44
10	5.89	TS[b]	TS[b]	6.07	−0.18	5.96	−0.07	5.76	0.13
11	5.85	5.40	0.45	5.43	0.42	5.57	0.28	5.97	−0.12
12	5.75	5.73	0.03	5.52	0.23	5.38	0.38	5.48	0.27
13	5.68	4.97	0.69	4.94	0.75	4.96	0.73	4.96	0.72
14	5.65	4.96	0.69	5.17	0.48	5.05	0.60	4.54	1.11
15	5.52	5.33	0.19	5.68	−0.16	5.39	0.13	5.30	0.22
16	5.49	TS[b]	TS[b]	5.37	0.12	5.46	0.03	5.41	0.08
17	5.27	5.53	−0.26	5.20	0.07	5.78	−0.51	5.18	0.09
18	5.08	5.30	−0.22	5.25	−0.17	4.86	0.22	5.17	−0.09
19	4.95	4.71	0.24	4.84	0.11	4.89	0.05	4.80	0.15
20	4.91	TS[b]	TS[b]	5.15	−0.24	5.20	−0.29	5.35	−0.44
21	4.89	5.49	−0.60	5.79	−0.90	5.72	−0.83	5.68	−0.80
22	4.86	4.92	−0.06	4.66	0.20	4.70	0.16	5.10	−0.24
23	4.82	5.18	−0.36	5.09	−0.27	4.93	−0.11	4.73	0.09
24	4.80	3.53	1.27	3.83	0.97	3.74	1.06	3.41	1.39
25	4.60	5.43	−0.83	5.97	−1.37	5.13	−0.53	5.85	−1.25
26	4.52	4.53	−0.01	5.09	−0.57	4.62	−0.10	5.90	−1.38
27	4.49	TS[b]	TS[b]	5.43	0.94	5.38	−0.89	5.70	−1.21
28	4.48	6.05	−1.57	5.11	−0.63	5.45	−0.97	5.28	−0.80
29	4.43	4.71	−0.28	4.84	−0.41	5.01	−0.58	5.05	−0.62
30	4.29	4.21	0.08	5.39	−1.10	5.21	−0.92	5.06	−0.77
31	4.29	5.24	-0.95	4.57	-0.28	4.43	−0.14	4.62	−0.33
32	4.25	4.56	-0.31	4.39	-0.14	4.48	−0.23	4.12	0.13
33	4.04	4.33	-0.29	4.10	−0.06	4.09	−0.05	5.40	−1.35
34	4.00	3.46	0.54	3.68	0.32	3.48	0.51	3.90	0.10
35	3.71	TS[b]	TS[b]	2.91	0.80	2.85	0.86	3.77	−0.06
36	3.64	4.45	−0.81	3.97	−0.33	4.24	−0.60	4.25	−0.61
37	3.43	5.23	−1.80	5.14	−1.71	4.83	−1.40	4.43	−1.00
38	3.43	3.29	0.14	3.39	0.04	3.43	0.00	5.03	−1.60
39	3.22	4.97	−1.75	4.10	−0.88	4.52	−1.30	5.66	−1.44
40	2.80	3.64	−0.84	3.43	−0.63	3.33	−0.53	2.88	−0.08
42	2.64	2.34	0.30	2.34	0.30	2.30	0.34	2.09	0.55
46	4.07	4.67	−0.60	4.75	−0.69	4.78	−0.71	4.78	−0.71
47	4.03	3.35	0.68	3.37	0.66	3.48	0.55	2.78	1.25
48	3.84	4.28	−0.44	4.01	−0.17	3.99	−0.15	3.96	−0.12
49	3.88	TS[b]	TS[b]	4.21	−0.33	4.15	−0.27	4.12	−0.25
50	3.72	6.25	−2.53	3.35	0.37	3.63	0.09	3.84	−0.12
51	3.73	TS[b]	TS[b]	4.54	−0.81	4.93	−1.21	5.06	−1.33

Table 3. Continued.

Compound[a]	Experimental pK_i^{app}	Group 1 CoMFA		Group 2 CoMFA		Group 3 CoMFA		Group 3 CoMSIA	
		pK_i^{app}	Residual	pK_i^{app}	Residual	pK_i^{app}	Residual	pK_i^{app}	Residual
52	3.57	4.62	−1.05	4.10	−0.53	4.32	−0.75	2.98	0.59
53	3.43	TS[b]	TS[b]	3.38	0.05	3.48	−0.05	5.67	−2.24
54	3.22	TS[b]	TS[b]	4.06	−0.84	4.19	−0.97	3.25	−0.03
55	3.05	4.68	−1.63	2.91	0.14	3.70	−0.66	3.59	−0.54
61	4.65	4.99	−0.34	4.94	−0.29	4.87	−0.22	4.45	0.20
62	4.50	3.97	0.53	3.74	0.76	4.03	0.47	3.72	0.78
63	3.74	4.40	−0.66	4.46	−0.72	4.04	−0.30	4.55	−0.81
65	3.70	2.63	1.07	3.13	0.57	2.47	1.23	2.90	0.80
66	3.22	4.67	−1.45	3.83	−0.61	4.17	−0.95	3.98	−0.76
68	3.53	3.45	0.08	1.75	1.78	2.00	1.53	1.57	1.96
69	2.92	TS[b]	TS[b]	4.00	−1.08	4.62	−1.70	4.81	−1.89
71	7.79	7.77	0.02			7.69	0.10	7.01	0.78
72	8.08	4.19	3.89			5.52	2.56	6.58	1.49
73	7.84	TS[b]	TS[b]			6.74	1.10	7.12	0.72
74	7.28	6.96	0.32			7.89	−0.61	6.84	0.44
75	8.05	6.93	1.12			6.95	1.10	6.64	1.41
76	7.97	7.03	0.94			7.90	0.07	8.43	−0.46
77	7.00	TS[b]	TS[b]			6.18	0.82	6.75	0.25
78	7.40	TS[b]	TS[b]			7.01	0.39	6.32	1.08
79	7.22	5.28	1.94			5.11	2.11	6.98	0.24
80	6.50	5.17	1.33			4.76	1.73	6.08	0.42

[a]Compounds 71–80 represent bensulfuron methyl, chlorimuron ethyl, chlorsulfuron, ethametsulfuron methyl, ethoxysulfuron, metsulfuron methyl, pyrazosufuron ethyl, sulfometuron methyl, thifensulfuron methyl and tribenuron methyl respectively.
[b]TS = test set compounds. An accurate pK_i^{app} could not be determined for compounds 41, 43, 44, 45, 56, 57, 58, 59, 60, 64 and 67 (see text). The predicted sum of squares values ($\Sigma(Y_{obs} - Y_{pred})^2$) for group 1 by CoMFA is 57.42, for group 2 by CoMFA is 25.60, for group 3 by CoMFA is 45.28 and for group 3 by CoMSIA is 51.93.

structural terms, as the derived models are not always based on the bioactive conformation of a particular scaffold. Here, we plotted the various fields of CoMFA or CoMSIA based models on the sulfonylurea binding site of yeast AHAS to interpret the results. These superimpositions are shown in Figures 7 and 8.

For the CoMFA models, the cross-validated q^2 values of Group 2 and Group 3 were much higher than that for Group 1. Therefore, the Group 2 and Group 3 analyses were investigated further for their distributions of steric and electrostatic fields in space for residues within 5.5 Å of the center of the ligand. 3D contour maps from both training sets exhibited strong similarities except for the steric field (Figures 7a and 7c) near the heterocycle position. This is not surprising because Group 3 included 10 commercial sulfonylureas with substituents at both *meta* positions of the heterocycle while Group 2 only dealt with the monosubstituted series. For the steric fields, green shows positions where introducing a bulky group in a sulfonylurea would be favorable for greater inhibition of AHAS. In contrast, yellow indicates positions where decreasing the bulk of the sulfonylurea is favored. The steric fields indicate that the green regions are located in the cavities formed by: (a) Val583, Trp586 and Met582; (b) Ala117, Val191 and Lys251; (c) Ala200, Phe201 and Asp379; and (d) a fairly vacant space near the methoxy group of chlorimuron ethyl. The yellow regions are situated in spaces where bulky conflicts occur (near Val583, Trp586 and Asp379) and weaken the binding. For the electrostatic fields (Figure 7b and d), blue regions indicate areas where positive charges are favored for increased binding to the enzyme and red regions indicate spaces where negative charges are advantageous for the activity of sulfonylureas. As shown by these electrostatic fields, sulfonylureas need contributions from positively charged

Table 4. PLS statistics of 3D-QSAR models for inhibitory activities for sulfonylureas.

PLS statistics	CoMFA			CoMSIA
	Group 1	Group 2	Group 3	Group 3
q^2	0.459	0.611	0.673	0.644
Components	7	8	8	8
r^2	0.966	0.959	0.974	0.931
S	0.283	0.233	0.248	0.409
F	181.34	145.012	281.559	99.106
Contribution				
Steric	0.533	0.600	0.550	0.215
Electrostatics	0.467	0.400	0.450	0.324
Hydrophobic				0.338
H-bond acceptor				0.123

groups to achieve enhanced inhibition in most areas of the electrostatic field, and only small portions prefer negative charges. In the binding site of yeast AHAS, Asp379 has a negative charge, the side-chains of Lys251 and Arg380 are positive, and all other amino acids bear no charge. There is no obvious relationship between the electrostatic fields and herbicide-binding site for the CoMFA results shown here. If the structure of *Arabidopsis thaliana* AHAS had been available and partial charges were used for the active site (as suggested by a reviewer) then a correlation may have been obtained. However, the two electrostatic maps from Group 2 and Group 3 share significant similarity and the models are still useful for novel sulfonylurea design and interpretation of the 3D-QSAR models.

To understand the enzymatic activities of sulfonylureas in relation to their hydrophobic and H-bonding properties, the 3D-QSAR models from the CoMSIA analysis mentioned above were

Table 5. Obtained q^2 values for the 31 possible combinations of the property fields considered in CoMSIA for group 2 and group 3.

Combination	Group 2		Group 3		Combination	Group 2		Group 3	
	q^2	*n*	q^2	*n*		q^2	*n*	q^2	*n*
r	0.458	8	0.586	7	*r*, *q*, *d*	0.384	2	0.585	6
q	0.398	5	0.522	6	*r*, *q*, *a*	0.366	4	0.582	6
l	0.273	5	0.488	6	*r*, *l*, *d*	0.415	3	0.545	5
d	0.275	3	0.093	2	*r*, *l*, *a*	0.322	9	0.595	10
a	0.340	4	0.375	6	*r*, *d*, *a*	0.352	3	0.578	6
r, *q*	0.417	9	0.614	6	*q*, *l*, *d*	0.415	3	0.460	5
r, *l*	0.371	9	0.574	5	*q*, *l*, *a*	0.325	7	0.559	6
r, *d*	0.360	9	0.600	8	*q*, *d*, *a*	0.352	3	0.458	5
r, *a*	0.346	4	0.545	4	*l*, *d*, *a*	0.429	3	0.417	5
q, *l*	0.328	7	0.591	7	*r*, *q*, *l*, *d*	0.405	3	0.563	5
q, *d*	0.366	2	0.464	6	*r*, *q*, *l*, *a*	0.348	5	0.644	8
q, *a*	0.307	6	0.505	4	*r*, *q d*, *a*	0.368	3	0.558	4
l, *d*	0.414	3	0.297	5	*r*, *l*, *d*, *a*	0.412	3	0.566	5
l, *a*	0.322	7	0.440	7	*q*, *l*, *d*, *a*	0.371	3	0.491	5
d, *a*	0.306	4	0.334	4	*r*, *q*, *l*, *d*, *a*	0.374	4	0.573	5
r, *q*, *l*	0.367	9	0.612	8					

r, q, l, d, and a represent the steric, electrostatic, hydrophobic, and hydrogen-bond donor and acceptor property fields respectively.

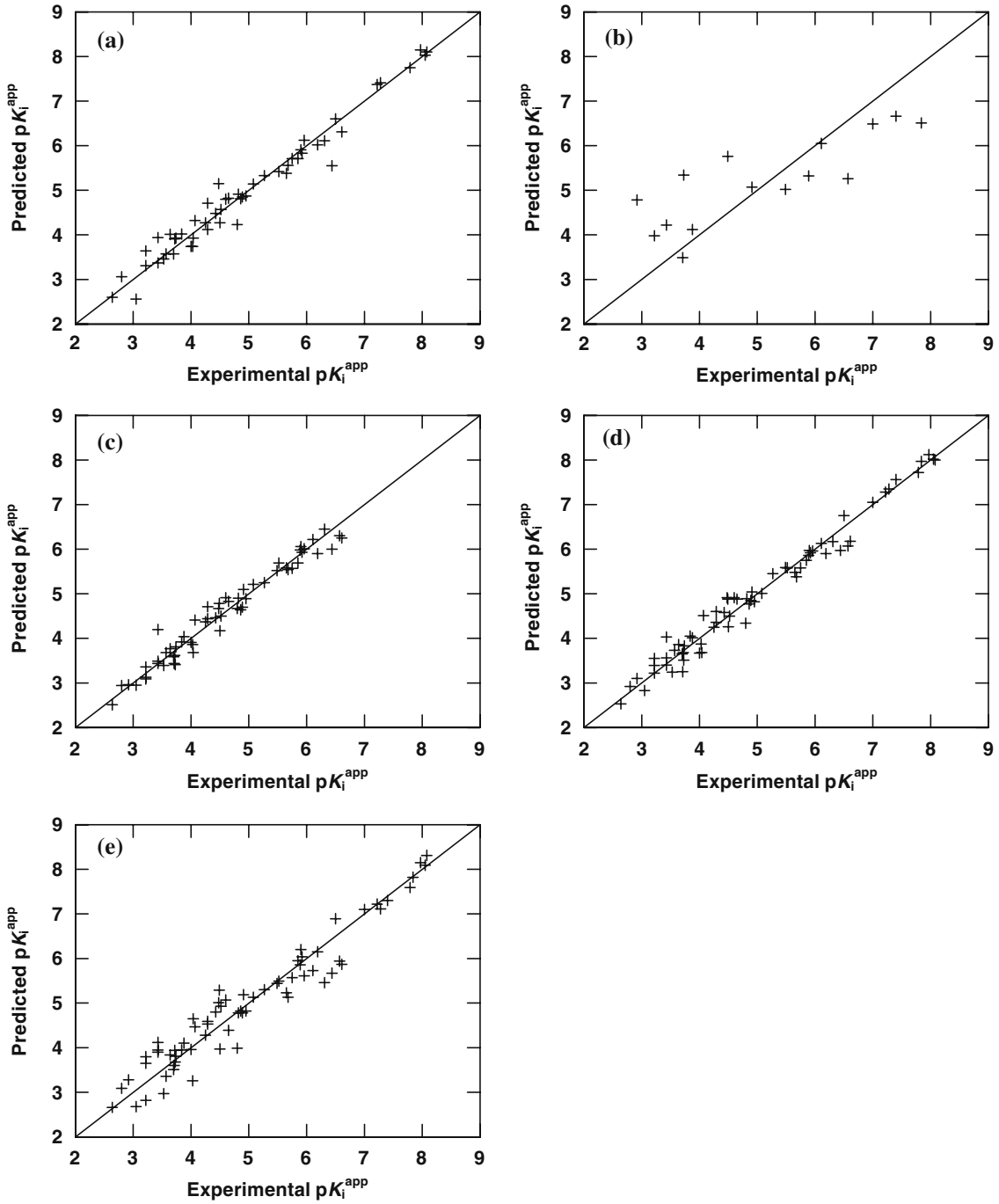

Figure 6. Predicted *versus* experimental activities of sulfonylureas. The training sets were: Panel (a), CoMFA analysis for Group 1; Panel (c), CoMFA analysis for Group 2; Panel (d), CoMFA analysis for Group 3; Panel (e), CoMSIA analysis for Group 3. The test set of CoMFA analysis for Group 1 is shown in Panel (b). The squared correlation coefficients (r^2) for the CoMFA training sets are 0.966 (Group 1), 0.959 (Group 2), 0.974 (Group 3), while that for the CoMSIA analysis of Group 3 is 0.931. The squared correlation coefficient for the test set is 0.687 (Panel b), showing the predictive ability of the 3D-QSAR model.

Table 6. Herbicidal activity of monosubstituted sulfonylureas.

Compound[a]	IC_{50} (M)
SM[b]	$2.81 \pm 0.16 \times 10^{-8}$
1	$4.89 \pm 0.50 \times 10^{-7}$
2*	$5.22 \pm 0.29 \times 10^{-7}$
3	$3.15 \pm 0.77 \times 10^{-7}$
4*	$6.00 \pm 1.04 \times 10^{-7}$
5*	$2.43 \pm 0.23 \times 10^{-5}$
6	$1.33 \pm 0.15 \times 10^{-6}$
7	$2.26 \pm 0.35 \times 10^{-5}$
8	$2.35 \pm 0.23 \times 10^{-6}$
9	$3.12 \pm 0.63 \times 10^{-6}$
10	$4.41 \pm 0.85 \times 10^{-6}$
11	$3.44 \pm 0.35 \times 10^{-6}$
12	$1.04 \pm 0.13 \times 10^{-5}$
13*	$5.54 \pm 1.00 \times 10^{-6}$
14	$1.93 \pm 0.23 \times 10^{-4}$
15	$1.69 \pm 0.17 \times 10^{-5}$
16	$5.68 \pm 0.81 \times 10^{-6}$
17	$1.22 \pm 0.30 \times 10^{-4}$
18	$1.47 \pm 0.38 \times 10^{-4}$
19*	$1.23 \pm 0.15 \times 10^{-4}$
31*	$4.05 \pm 0.30 \times 10^{-5}$
36*	$7.18 \pm 0.61 \times 10^{-4}$
38*	$9.15 \pm 4.70 \times 10^{-4}$
40*	$3.94 \pm 0.07 \times 10^{-4}$
42*	$3.34 \pm 0.42 \times 10^{-4}$

[a]Compounds marked with an asterisk belong to the R_1 = CO–OC_2H_5 series.
[b]SM = sulfometuron methyl.

plotted to represent the contribution by steric, electrostatic, hydrophobic and H-bond acceptor fields. Because CoMSIA analysis does not have a requirement for an energy cutoff to calculate the fields, the steric and electrostatic fields displayed using CoMSIA are clearer than the corresponding CoMFA maps for Group 3. For the steric map (Figure 8a), the green region segregates into three parts to fit the cavities formed by: (a) Val583, Trp586 and Met582; (b) Ala117, Val191 and Lys251; and (c) the space around the methoxy group of the heterocycle. The yellow contours are in regions where steric clashes with Val583, Gly116 and Ala117 might decrease the binding affinity. The results are in good accordance with those observed in CoMFA. For the electrostatic field of CoMSIA (Figure 8b), a better relationship between the binding site and the electrostatic field distribution could be observed. Near the negatively charged Asp379, a positively charged group in a sulfonylurea will increase the inhibition and a negatively charged substituent near Arg380 is favorable for tighter binding. The hydrophobic interactions (Figure 8c) could be explained based on the hydrophobic force fields for CoMSIA models. In regions where yellow contours appeared, introduction of more hydrophobic groups leads to more potent inhibition of AHAS. These occurred in spaces near: (a) Trp586, Met582 and Gly116; or (b) near Val191 and Pro192. These residues have been shown previously [17] to make hydrophobic contacts with sulfonylureas. The gray region shows where a less hydrophobic substituent could give better inhibition, and is in a large vacant space where no interactions occur. Judging from the correlation of the hydrophobic field distribution and the schematic diagram of the binding site of chlorimuron ethyl–AHAS complex, the current CoMSIA model seems quite successful because hydrophobic interactions play a major role in ligand-enzyme binding. For the H-bond acceptor field (Figure 8d), the CoMSIA model was not in unambiguous agreement with the binding mode of a sulfonylurea to yeast AHAS [7], where Lys251 and Arg380 are involved as intermolecular H-bond donors. In the H-bond acceptor fields, the binding affinity will be increased if an H-bond acceptor group on the ligand (or an H-bond donor group on the receptor) is introduced in the magenta region; however, the inhibition will be weaker if such a new group is placed in the red area. The plot of H-bond acceptor field did not match the binding site well.

From the 3D-QSAR analyses, steric and hydrophobic fields show significant correlation with the binding site of yeast AHAS. All the models highlighted the importance of these factors for improved potency of sulfonylureas. Electrostatic and H-bond acceptor contributions also play important roles as structural features of herbicidal sulfonylureas, despite the fact that these fields did not fit perfectly with the yeast AHAS binding site.

Herbicidal activity

Over the past decade, we have tested compounds **1** to **69** and many others for herbicidal activity. However, these experiments have varied in the protocols, conditions, plant species and so on, making it more complex to compare the results directly. Nevertheless, these *in vivo* tests have

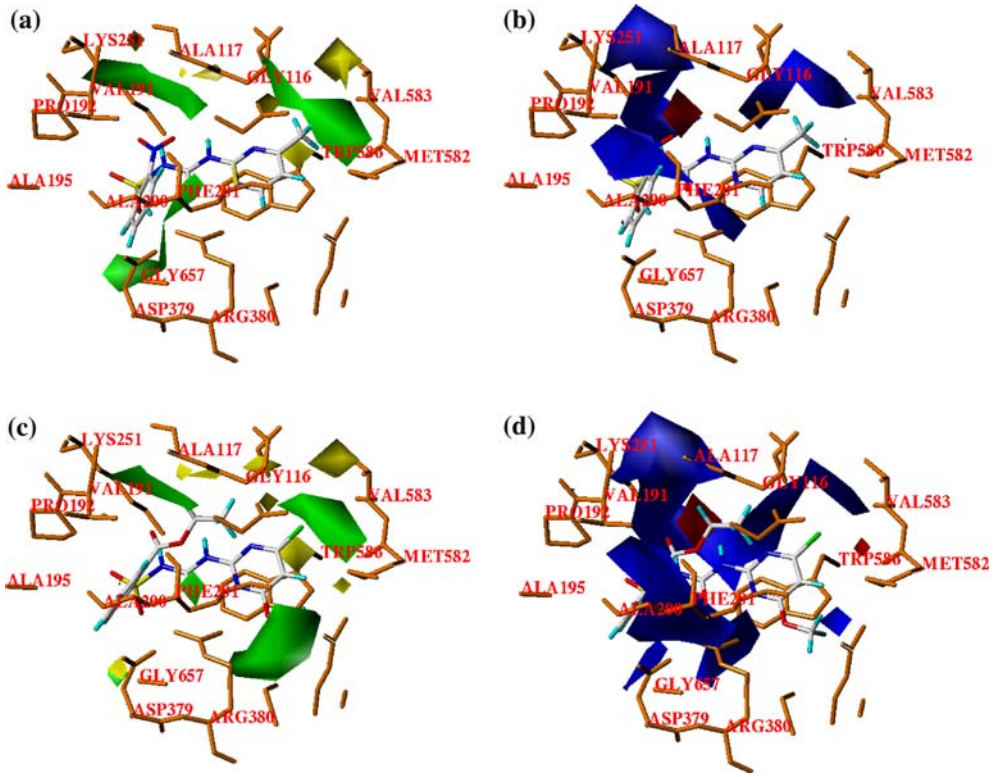

Figure 7. Contour plots from the final CoMFA analyses mapped on to the binding site of yeast AHAS [7]. Panels (a) and (b): Group 2 (monosubstituted sulfonylureas) with monosulfuron shown as a reference. Panels (c) and (d): Group 3 (all sulfonylureas) with chlorimuron ethyl shown as a reference. For the steric field contour maps (Panels a and c), yellow contours (20%) indicate regions where steric bulk decreases biological activity and green contours (80%) indicate regions where steric bulk increases activity. For the electrostatic field contour maps (Panels b and d), blue (80%) and red (20%) regions indicate where biological activity is enhanced by positive and negative charge, respectively.

shown that monosulfuron (**1**) is an effective herbicide and it is of interest that this compound is the most potent of the monosubstituted sulfonylureas as an AHAS inhibitor. Based on this result, we tested under uniform conditions a selected subset of compounds as herbicides to determine whether *in vitro* inhibition of AHAS is a good predictor of *in vivo* herbicidal activity. For these experiments we chose two groups of compounds: those that are the most potent, with an apparent K_i value of less than 10 μM (Table 2, compounds **1**–**18**); and the series where R_1 is $CO–OC_2H_5$ while R_2 is varied (Table 2, compounds **2**, **4**, **5**, **13**, **19**, **31**, **36**, **38**, **40** and **42**). This latter group covers a very wide range of apparent K_i values, from less than 0.3 μM (compound **2**) to over 2 mM (compound **42**). For comparison, one of the commercial sulfonylureas (sulfometuron methyl, K_i^{app} = 40 nM) was also included in the former experiment. Representative herbicidal activity data (compound **13**, which is a member of both series tested) are shown in Figure 9a yielding an IC_{50} value of 5.54 μM. While this is higher than the apparent K_i (2.07 μM), the agreement is quite good bearing in mind the enormous difference between an experiment on a pure enzyme and one using growing seedlings.

IC_{50} values for all compounds tested are shown in Table 6. There is a strong correlation between the inhibition of AHAS *in vitro* and the *in vivo* herbicidal activity, as illustrated in Figure 9b (low apparent K_i series) and Figure 9c (R_1 = $CO–OC_2H_5$ series). This correlation demonstrates that herbicidal activity of these compounds is mainly or solely due to inhibition of AHAS and that the K_i value measured *in vitro* is a useful predictor of their effect *in vivo*.

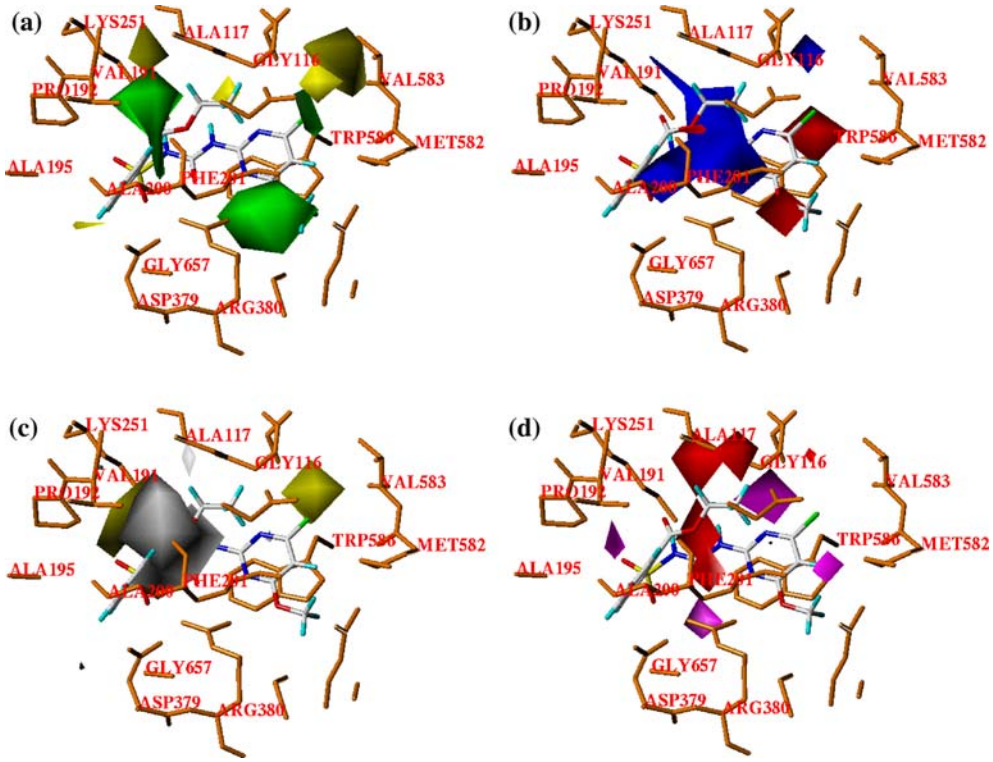

Figure 8. Contour plots from the final CoMSIA analysis for group 3 mapped on to the binding site of yeast AHAS [7], with chlorimuron ethyl shown as a reference. Panel (a), steric contour map; green contours (80%) indicate regions where steric bulk is favored for biological activity and yellow contours (20%) indicate regions where steric bulk is disfavored for activity. Panel (b), electrostatic contour map; positive charge is required in blue (80%) regions and negative charge is required in red (20%) regions to improve activity. Panel (c), hydrophobic contour map; hydrophobic groups (yellow, 80%) and hydrophilic groups (gray, 20%) will increase activity. Panel (d), H-bond acceptor contour map; magenta (80%) and red (20%) contours show regions where hydrogen bond donor groups in the binding site increase and decrease inhibitory activity, respectively.

Conclusions

The development of AHAS inhibitors as practical herbicides has never proceeded on a rational basis. Sulfonylureas and another major family of AHAS-inhibiting herbicides, the imidazolinones [32], were both shown to be effective *in vivo* well before their enzymatic target was identified. Similarly, the molecular variations that result in useful herbicides (e.g. Table 1) were discovered by extensive programs of chemical synthesis rather than from knowledge of the structure of the herbicide-binding site. The structural rules developed by Levitt and coworkers [33] for the sulfonylureas have been valuable, but they are not immutable laws. This is clearly exemplified by monosulfuron, which does not conform to the rule that the heterocyclic ring must be substituted in both *meta* positions. Despite this structural variation, monosulfuron is an effective herbicide (Table 6) and a strong inhibitor of plant AHAS (Figure 2). Furthermore, monosulfuron has been shown to be an effective herbicide for weed control in millet in Northern China, while other disubstituted sulfonylureas are non-selective herbicides for this crop (unpublished data).

Here we show that monosulfuron is not unique in this respect and that a variety of other monosubstituted sulfonylureas will inhibit AHAS (Table 2). For high potency AHAS inhibition, the sole heterocyclic substituent should be small and hydrophobic while the *ortho* substituent on the aromatic ring should be small and polar (Table 2). Compounds with more radical departures in structure from those of conventional sulfonylureas are generally ineffective inhibitors (Figrues 3 and 4). There is a strong correlation between potency of AHAS inhibition and herbicidal activity (Figure 9).

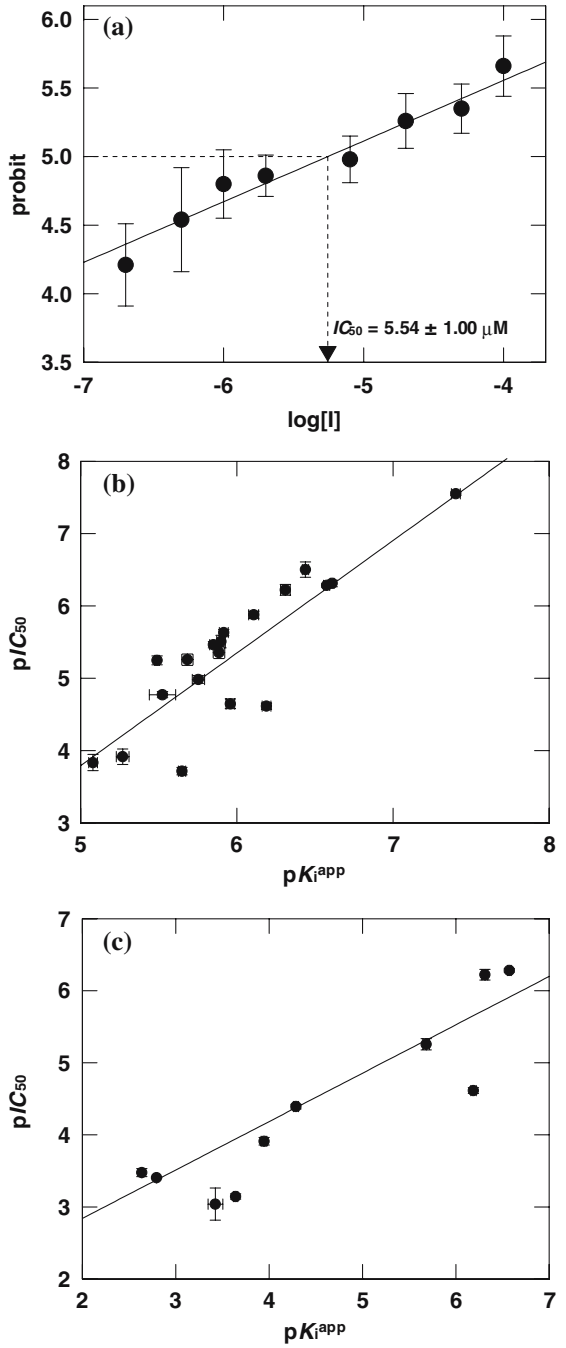

Figure 9. Herbicidal activity of sulfonylureas. Panel (a) shows the analysis of the inhibition by compound **13** of rape seed root growth. The IC_{50} of 5.54 ± 1.00 μM is calculated as the concentration that gives a probit of 5.0. Panels (b) (low apparent K_i series) and (c) (R_1 = CO–OC_2H_5 series) illustrate the correlation between the IC_{50} measured *in vivo* and the K_i value for inhibition of AHAS *in vitro*; the data are plotted on negative logarithmic scales on both axes. The regression equation for the data in panel (b) is slope = 1.556 ± 0.166, intercept = −3.988 ± 1.055, r^2 = 0.916, while that for panel (c) is slope = 0.672 ± 0.076, intercept = 1.497 ± 0.270, r^2 = 0.953.

3D-QSAR techniques have demonstrated their abilities to explain the different affinities of 68 herbicidal sulfonylureas for *A. thaliana* AHAS. Excellent cross-validated q^2 and non-cross-validated r^2 were obtained for both CoMFA and CoMSIA analyses. The activity of a test set with 15 molecules was estimated fairly accurately from the analysis (with r^2_{pred} of 0.687), indicating that the alignment of the molecules was valid. For different training sets, CoMFA and CoMSIA gave similar correlations of inhibitory data and steric and electrostatic fields and CoMSIA suggested steric, electrostatic, hydrophobic and H-bond acceptor requirements for increased potency of this class of inhibitors. When superimposing the resulting 3D contour maps on to the herbicide-binding site of yeast AHAS, a very good correlation was observed between the surrounding residues and the shapes of steric and hydrophobic fields, which again proved the validity of the models. The final 3D-QSAR plots enhance the understanding of ligand binding and the necessary structural features of sulfonylurea herbicides. The resulting models allow the prediction of inhibition constants of novel sulfonylureas and provide a new opportunity for guiding optimization of the structures to accelerate the discovery of compounds with high biological activity.

Acknowledgement

This work was supported by the Linkage-International Program of the Australian Research Council (grant number LX0349233), National 973 Project of China (grant number 2003CB114406), the Natural Science Foundation Key Project of China (grant number 20432010), and the International Collaborative Key Project of Science and Technology Ministry of China (grant number 2004DFA01500).

References

1. Beyer, E.M. Jr, Duffy, M.J., Hay, J.V. and Schleuter D.D., In Kearney, P.C. and Kaufman, D.D., (Eds), Chemistry, Degradation and Mode of Action, Vol. 3, Marcel Dekker Inc. New York, NY, 1988, pp. 117–189.
2. Sauers, R.F. and Levitt, G., In Magee, P.S., Kohn, G.K. and Menn, J.J. (Eds.), Pesticide Synthesis Through Rational Approaches American Chemical Society Washington, DC, USA, 1984, pp. 21–28.

3. LaRossa, R.A. and Schloss, J.V., J. Biol. Chem., 259 (1984) 8753.
4. Ray, T.B., Plant Physiol., 75 (1984) 827.
5. Duggleby, R.G. and Pang, S.S., J. Biochem. Mol. Biol., 33 (2000) 1.
6. Pang, S.S., Duggleby, R.G. and Guddat, L.W., J. Mol. Biol., 317 (2002) 249.
7. Pang, S.S., Guddat, L.W. and Duggleby, R.G., J. Biol. Chem., 278 (2003) 7639.
8. McCourt, J.A., Pang, S.S., Guddat, L.W. and Duggleby, R.G., Biochemistry, 44 (2005) 2330.
9. Li, Z.-M., Jia, G.-F., Wang, L.-X., Fan, C.-W. and Yang, Z., Sulfonylurea compounds and their herbicidal applications. (1998) Chinese Invention Patent ZL 94–1–18793.4.
10. Wang, L.-X., Li, Z.-M., Jia, G.-F., Chen, J.-P. and Wang, S-H. The application of monosulfuron in millet fields. (2003) Chinese Invention Patent ZL 98–1–00257.9.
11. Li, Z.-M., Jia, G.-F., Wang, L.-X., Lai, C.-M., Wang, H.-G. and Wang, R.-J., Chem. J. Chin. Univ.-Chin., 14 (1993) 349.
12. Ye, G.-Z., Fan, Z.-J., Li, Z.-M., Li, Y.-H., Gao, F.-W. and Wang, S.-H., Chem. J. Chin. Univ.-Chin., 24 (2003) 1599.
13. Chang, A.K. and Duggleby, R.G., Biochem. J., 327 (1997) 161.
14. Sambrook, J., Fritsch, E.F. and Maniatis, T. Molecular Cloning: A Laboratory Manual , 2nd ed., Cold Spring Harbor Laboratory Press, Cold Spring Harbor, New York, USA, 1989.
15. Singh, B.K., Stidham, M.A. and Shaner, D.L., Anal. Biochem., 171 (1988) 173.
16. Inamori, Y., Muro, C., Yamanaka, H., Osaka, K., Hachiken, H., Tsujibo, H. and Miki, Y., Biosci. Biotech. Biochem., 58 (1994) 1150.
17. Chang, A.K. and Duggleby, R.G., Biochem. J., 333 (1998) 765.
18. Brown, H.M., Pestic. Sci., 29 (1990) 263.
19. Akagi, T., Pestic. Sci., 47 (1996) 309.
20. Liu, J., Li, Z.-M., Wang, X., Ma, Y., Lai, C.-M., Jia, G.-F. and Wang, L.-X., Sci. China, Ser., B41 (1998) 50.
21. Yang, G.-F., Liu, H.-Y., Yang, X.-F. and Yang, H.-Z., Sci. China, Ser., B42 (1999) 656.
22. Yang, G., Liu, H. and Yang, H., Pestic. Sci., 55 (1999) 1143.
23. Hou, T.J., Li, Z.M., Li, Z., Liu, J. and Xu, X.J., J. Chem. Inf. Comput. Sci., 40 (2000) 1002.
24. Ren, T.-R., Yang, H.-W., Gao, X., Yang, X.-L., Zhou, J.-J. and Cheng, F.-H., Pest Manage. Sci., 56 (2000) 218.
25. Li, Z.-M. and Lai, C.-M., Chin. J. Org. Chem., 21 (2001) 810.
26. Galeazzi, R., Marucchini, C., Orena, M. and Zadra, C., Bioorg. Med. Chem., 10 (2002) 1019.
27. Cramer, R.D. III, Paterson, D.E. and Bunce, J.D., J. Am. Chem. Soc., 110 (1988) 5959.
28. Klebe, G., Abraham, U. and Mietzner, T.J., Med. Chem., 37 (1994) 4130.
29. Klebe, G., In Kubinyi, H., Folkers, G. and Martin, Y.C. (Eds.) 3D QSAR in Drug Design Vol 3: Recent Advances. Kluwer Academic Publishers, Dordrecht, The Netherlands, 1998, pp. 87–105.
30. Pang, S.S., Guddat, L.W. and Duggleby, R.G., Acta Cryst., D60 (2004) 153.
31. Duggleby, R.G., Pang, S.S., Yu, H. and Guddat, L.W., Eur. J. Biochem., 270 (2003) 2895.
32. Los, M., In Magee, P.S., Kohn, G.K. and Menn, J.J. (Eds.) Pesticide Synthesis Through Rational Approaches. American Chemical Society, Washington, DC, USA, 1984, pp. 29–44.
33. Levitt G., In Baker D.R., Fenyes J.G., Moberg W.K., (eds.), 1991, *Synthesis and Chemistry of Agrochemicals II*. ACS Symposium Series 443 (American Chemical Society Washington DC, USA) pp. 16–31.